

Title: Stochasticity in Ca^{2+} increase in spines enables robust and sensitive information coding

Authors: Takuya Koumura^{1†}, Hidetoshi Urakubo^{2††}, Kaoru Ohashi², Masashi Fujii² and Shinya Kuroda^{1,2*}

Affiliations: ¹Undergraduate Department of Bioinformatics and Systems Biology, ²Department of Biophysics and Biochemistry, Graduate School of Science, University of Tokyo, Hongo 7-3-1, Bunkyo-ku, Tokyo 113-0033, Japan.

†Present address: Department of Life Sciences, Graduate School of Arts and Sciences, University of Tokyo, Komaba 3-8-1, Meguro-ku, Tokyo 153-8902, Japan.

††Present address: Department of Systems Science, Graduate School of Informatics, Kyoto University, Uji 611-0011 JAPAN

Running head: Probabilistic coding of Ca^{2+} increase in spines

* **E-mail:** skuroda@bi.s.u-tokyo.ac.jp

ABSTRACT

A dendritic spine is a very small structure ($\sim 0.1 \mu\text{m}^3$) of a neuron that processes input timing information. Why are spines so small? Here, we provide functional reasons; the size of spines is optimal for probability coding of Ca^{2+} increases, which makes robust and sensitive to input timing information. We created a stochastic simulation model of input timing-dependent Ca^{2+} increases in a cerebellar Purkinje cell's spine. Spines used probability coding of Ca^{2+} increases rather than amplitude coding for input timing detection via stochastic facilitation by utilizing the small number of molecules in a spine volume, which appeared optimal for probability coding. Probability coding of Ca^{2+} increases in a spine volume was more robust against input fluctuation and more sensitive to input numbers than amplitude coding of Ca^{2+} increases in a cell volume. Thus, stochasticity is a strategy by which neurons robustly and sensitively code information.

AUTHOR SUMMARY (100-200 words, 153 words)

A spine is a small platform ($0.1 \mu\text{m}^3$, 10^4 -fold smaller than a cell) for information processing in a neuron. Signal transmission in a spine inevitably becomes noisy due to low numbers of molecules in a small volume. The noise generally perturbs signal transmission, but how can a spine accurately receive input information under such noisy conditions? Here we show that a spine utilizes noise-enhancing signal transmission termed as ‘probability coding’ resulting from the smallness of a spine, and the spine volume appeared ‘optimal’ for the probability coding. In the stochastic simulation of Ca^{2+} increases in various volumes, the spine volume preferred the ‘probability coding’, whereas the cell volume preferred the general ‘amplitude coding’. We found that the ‘probability coding’ was much more robust against noise, and has the higher information per volume. These findings clearly demonstrate the advantage of smallness and numerosity of spines in information processing, especially for signals of synaptic plasticity.

INTRODUCTION

A dendritic spine is a small structure on the dendrites of a neuron that processes input timing information from other neurons, and typically, tens to hundreds of thousands of spines are present on a neuron [1,2]. Small volumes and large numbers are representative characteristics of spines. For example, the volume of the spines at the parallel fibre (PF)-cerebellar Purkinje cell synapse is approximately $0.1 \mu\text{m}^3$ [3], which is 10^4 -fold smaller than the cell body ($5,000 \mu\text{m}^3$) [4,5], and 175,000 spines are present on a single neuron (**Fig. 1A**) [1]. Cerebellar Purkinje cells receive two inputs: PF inputs from granular neurons that are thought to code sensorimotor signals and a climbing fibre (CF) input from inferior olivary nucleus that is thought to code error signal [6,7,8]. The timing between the PF-CF activation has been shown to be important for associative eyelid conditioning in cerebellar learning [9,10]. Coincident PF and CF inputs but not PF or CF inputs alone to spines at the PF-Purkinje cell synapse induce large Ca^{2+} increases via IP_3 (inositol trisphosphate)-induced Ca^{2+} release (IICR) from intracellular Ca^{2+} stores, such as the endoplasmic reticulum (ER) [11,12] (**Fig. 1B**). Large Ca^{2+} increases subsequently trigger long-term decreases of synaptic strength that are known as cerebellar long-term depression (LTD) [13], which is thought to be the molecular and cellular basis of our motor learning [7].

Ca^{2+} increases depend on the relative timing of the PF and CF inputs, and the time window between PF and CF inputs that produces Ca^{2+} increases has been experimentally determined (**Fig. 1C**) [12]. Large Ca^{2+} increases occur only when PF and CF inputs are coincident at a given synapse within a 200 msec time window. We previously developed a deterministic kinetic model of PF and CF inputs-dependent Ca^{2+} increases based on experimental findings and reproduced the time window curve of the Ca^{2+} increase [14]. However, in a spine, the number of signaling molecules is limited to tens to hundreds (**Fig. 1B**); thus, reactions should fluctuate stochastically.

Indeed, experimentally, the same coincident PF and CF inputs do not always induce similar large Ca^{2+} increases; in some cases, large Ca^{2+} increases are observed, whereas in other cases, they are not (**Fig. 1C**) [12]. How can a spine robustly and sensitively code input timing information under such stochastic conditions with limited numbers of molecules [15,16,17]? To address this issue, we created a stochastic simulation model of input-timing-dependent Ca^{2+} increase in a spine volume based on the deterministic kinetic model of Ca^{2+} increase in a spine at the PF-Purkinje cell synapse [14] that incorporated stochastic reactions due to the small number of molecules.

RESULTS

Stochastic simulation of Ca^{2+} increase in a spine at the PF-Purkinje cell synapse

We used the same kinetic framework and parameters of PF and CF inputs-dependent Ca^{2+} increase in the stochastic simulation used in our previous deterministic model [14]: the PF inputs presynaptically released glutamate (**Fig. 1B**). Glutamate binds and activates metabotropic glutamate receptors (mGluRs), which leads to an increase in IP_3 . Glutamate also binds and activates α -amino-3-hydroxy-5-methyl-4-isoxazole propionic acid receptors (AMPA), which leads to an increase in Ca^{2+} influx through indirect activation of voltage-gated Ca^{2+} channels (VGCC). The CF input causes Ca^{2+} influx through VGCCs. The IP_3 receptor, an intracellular Ca^{2+} channel, is activated only when it binds simultaneously with both IP_3 and Ca^{2+} . When the ternary complex of $\text{Ca}^{2+}\cdot\text{IP}_3\cdot\text{IP}_3$ receptor is formed by the PF input, the Ca^{2+} influx via CF input triggers a positive feedback loop of Ca^{2+} -dependent Ca^{2+} release that leads to a large Ca^{2+} increase from intracellular Ca^{2+} stores, such as the ER. This large Ca^{2+} increase induces a delayed negative feedback inhibition of Ca^{2+} release from the stores at higher levels of Ca^{2+} . Therefore, PF and CF inputs-dependent Ca^{2+} increase is generated by positive- and delayed

negative-feedback loops. This forms a single, large and transient Ca^{2+} increase, depending on the relative timing of the PF and CF inputs.

We stochastically simulated the Ca^{2+} increase due to PF and CF inputs in a spine and in a cell volume (**Fig. 2, Fig. S1**). The volumes of spines and cells have been reported to be $0.1 \mu\text{m}^3$ [3] and $5,000 \mu\text{m}^3$ [4,5], respectively. We hereafter denote $0.1 \mu\text{m}^3$ as a spine volume and $5,000 \mu\text{m}^3$ as a cell volume. In response to coincident PF and CF inputs ($\Delta t = 160$ msec), a large Ca^{2+} increase was always observed in a cell volume (**Fig. 2A**, black lines). In a spine volume, a large Ca^{2+} increase was observed in many (1371 cases in 2000 trials) but not all cases (**Fig. 2A**, gray lines). In response to PF and CF inputs with reversed timing ($\Delta t = -400$ msec), no large Ca^{2+} increase was observed in a cell volume (**Fig. 2B**, black lines). In a spine volume, however, a large Ca^{2+} increase was observed in some cases (690 cases in 2000 trials), but not in many cases (**Fig. 2B**, gray lines). In both timing, the amplitudes of the Ca^{2+} increases fluctuated between trials in a spine volume, but not in a cell volume. Regardless of the input timing, Ca^{2+} increase occurred only once. We defined the integrated Ca^{2+} as the temporal integration of Ca^{2+} concentration, subtracted by the basal Ca^{2+} concentration. The probability distribution of the integrated Ca^{2+} in a spine volume appeared bimodal (**Fig. 2C**). The narrow mode on the left corresponds with trials of no Ca^{2+} increase, and the wide mode on the right corresponds with the trials with large Ca^{2+} increases. In response to coincident PF and CF inputs, the height of the right mode increased and that of the left mode decreased. The mean of each mode appeared similar, regardless of the timing between the PF and CF inputs. This finding suggests that in a spine volume, the timing information is encoded by the probability of a large Ca^{2+} increase (fraction of trials) rather than the amplitude of Ca^{2+} increase.

Probability coding of Ca^{2+} increase in a spine

We next examined the distribution of the integrated Ca^{2+} in every 20 msec PF-CF intervals between -400 msec and 600 msec in a spine volume (**Fig. 3A**, left panel). In all PF-CF intervals, the probability distribution of the integrated Ca^{2+} appeared bimodal. In the time window between 0 msec and $+340$ msec PF-CF intervals, the upper mode of the distribution appeared dominant. Outside of this time window, the lower mode of the distribution appeared dominant. Such bimodality was not observed at all in the distribution in a cell volume, where unimodality was always observed regardless of the PF-CF interval (**Fig. 3B**, left panel). In both a spine and a cell volume, however, the mean integrated Ca^{2+} showed similar graded bell-shaped curves (**Fig. 1C**). These results suggest that information of the PF-CF interval is coded by the probability of a large Ca^{2+} increase in a spine volume, and by the amplitude of a large Ca^{2+} increase in a cell volume.

Therefore, we examined whether the probability or amplitude of the Ca^{2+} increase codes the information on PF-CF interval by decomposing the distribution of the integrated Ca^{2+} into the probability and amplitude components (**Fig. 2D**, Materials and Methods). First, we determined the threshold between the two peaks of the marginal distributions (**Fig. 3**, arrowheads in left panels). Then, we divided the distribution by the threshold (i.e. distributions above or below the threshold). The probability component of the distribution was defined as the frequencies of the integrated Ca^{2+} in each divided distribution (**Fig. 2D**, middle panel). The amplitude component was defined as the distribution of the integrated Ca^{2+} in each divided distribution (**Fig. 2D**, bottom panel). The total distribution of the integrated Ca^{2+} (**Fig. 2D**, top panel) is the sum of the amplitude components weighted with the probability components (see Materials and Methods).

In a spine volume, the probability component of the integrated Ca^{2+} was graded bell-shaped curves along the PF-CF interval (**Fig. 3A**, middle panel), whereas the amplitude component of

the integrated Ca^{2+} was flat along the PF-CF interval (**Fig. 3A**, right panel). This result indicates that in the stochastic model in a spine volume, timing information between PF and CF inputs is coded by the probability component of the integrated Ca^{2+} rather than the amplitude component of the integrated Ca^{2+} .

In contrast, in a cell volume, the amplitude component of the integrated Ca^{2+} showed a graded bell-shaped curve along the PF-CF interval (**Fig. 3B**, right panel). However, the probability component of the integrated Ca^{2+} was a rectangular curve along the PF-CF interval (**Fig. 3B**, middle panel), meaning that the probability component can be used only to detect the binary input timing information on whether the input timing was inside or outside the time window; it cannot be used for the detection of the small input timing difference. In a volume smaller than a spine volume, both the probability and amplitude components were flat along the PF-CF interval (**Fig. 3C**, middle and right panels). These results suggest that the probability and amplitude components of the integrated Ca^{2+} are the dominant factor in the distribution of the integrated Ca^{2+} in a spine volume and in a cell volume, respectively.

We next quantified the input timing information coded by the distribution of the integrated Ca^{2+} , the probability components, and the amplitude components in a volume-dependent manner (**Fig. 3D**, **Fig. S2**). We first measured the total input timing information coded by the distribution of the integrated Ca^{2+} by mutual information between the integrated Ca^{2+} and PF-CF interval (**Fig. 3D**, black line). Then, we calculated the distribution without the probability component or amplitude component from the original distribution of the integrated Ca^{2+} (**Fig. S2**, **Materials and Methods**). We measured the information coded by the probability component by the Kullback–Leibler (KL) divergence of the probability component-removed distribution from the original distribution of the integrated Ca^{2+} (**Fig. 3D**, red line). Similarly, we measured the

information coded by the amplitude component by the KL divergence of the amplitude component-removed distribution from the original distribution of the integrated Ca^{2+} (**Fig. 3D**, blue line). The input timing information coded by the probability component, amplitude component, and original distribution increased monotonically as the volume became larger (**Fig. 3D**). As the volume increased, the information coded by the probability component gradually increased and converged to 1bit in a cell volume, indicating that a cell can discriminate binary information with the probability component (**Fig. 3D**, red line). The information coded by the amplitude component was lower than that coded by the probability component in a spine volume, and became larger than that coded by the probability component in the volume larger than $5 \mu\text{m}^3$ (**Fig. 3D**, blue line). The total information on input timing in a cell volume was larger than that in a spine volume; however, spines utilize their numerosity to increase the amount of the input timing information (see **Fig. 4**).

We examined the relative contribution of the probability or amplitude component to the total information (**Fig. 3E**). We divided the information coded by probability or amplitude component by the sum of them, which is equal to the total information. The contribution of the probability component was larger than that of amplitude component between 0.05 and $5 \mu\text{m}^3$. This result indicates that the volume of a spine ($0.1 \mu\text{m}^3$) appears optimal for maximising input timing information coded by the probability component. The contribution of the probability component became smaller than that of the amplitude component when a volume became larger than $5 \mu\text{m}^3$. This indicates that the probability coding was dominant in a spine because of the fluctuation of the reaction derived from the smallness of the spines. Therefore, the probability coding in this study could be one of stochastic facilitation, the phenomenon in which information transmission is enhanced by noise or fluctuation [18]. In contrast, in the volume larger than $5 \mu\text{m}^3$, the relative

contribution of the amplitude component became larger than that of the probability component, indicating that amplitude coding is more efficient. Thus, a spine codes input timing information by the probability component of the distribution of the integrated Ca^{2+} by utilising its smallness, and a cell codes input timing information by the amplitude component of the distribution. In addition, this suggests that the same IICR system, a Ca^{2+} increase generator, can switch between probability coding and amplitude coding for input timing detection depending on the volume. As volume in the stochastic simulation increased, the behaviour of the stochastic model became similar to that of the deterministic model, which has a volume that can be regarded as infinity. Indeed, the stochastic simulation in a cell volume ($5,000 \mu\text{m}^3$) showed almost the same response as the previous deterministic model (**Fig. 2A, B, Fig. S1**) [14]. Therefore, we hereafter used the deterministic model as the model in a cell volume.

Robust and sensitive information coding in a spine

Since glutamate release from PFs fluctuates between trials in the physiological condition [19], the Ca^{2+} increase should be affected by the fluctuation of the amplitude of PF inputs (PF amplitude). We simulated the Ca^{2+} increase with the fluctuation of PF amplitude between trials, and asked whether the probability coding in spines are advantageous for robust information coding on input timing against fluctuation of PF amplitude (**Fig. 4A-C**). Here we use the term “robustness” of information coding as invariability of input timing information against the increase of the fluctuation of PF amplitude. The means of the integrated Ca^{2+} in a spine volume (**Fig. 4A**) and in a cell volume (**Fig. 4B**) showed the similar graded bell-shaped curves, regardless of the coefficient of variation (CV) of the PF amplitude. However, the standard deviations of the integrated Ca^{2+} in a spine volume remained approximately the same regardless

of the CV values (**Fig. 4A**, dashed lines), whereas those in a cell volume became larger as the CV increased (**Fig. 4B**, dashed lines). These results suggest that input timing information coding is more robust in a spine volume than in a cell volume. Indeed, the input timing information coded by the integrated Ca^{2+} in a spine volume remained almost constant regardless of the CV of the PF amplitude (**Fig. 4C**, colored lines). Even in a single spine, the input timing information decreased only by 10.1% when the CV of the PF amplitude increased from 0.05 to 0.5 (**Table 1**). In contrast, the input timing information in a cell volume largely decreased as the CV of the PF amplitude increased (**Fig. 4C**, black line). The input timing information decreased by 77.3% when the CV of the PF amplitude increased from 0.05 to 0.5 (**Table 1**). These results indicate that spines utilize their smallness for the robust input timing information coding. The fluctuation in the amplitude of EPSPs has been reported to be 50% [19], which corresponds with a CV of 0.5. This fluctuation may be overestimated due to the inclusion of postsynaptic fluctuation; therefore, we used a CV of 0.1 for further study.

We also examined the sensitivity of the input timing information to the number of PF inputs in spines and in a cell (**Fig. 4F-F**). Here we use the term “sensitivity” of information coding as invariability of input timing information against the decrease of the number of PF inputs. The means of the integrated Ca^{2+} in a single spine showed a graded bell-shaped curve in response to 3-9 PF inputs (**Fig. 4D**), whereas the integrated Ca^{2+} in a cell showed the graded bell-shaped curve in response to 5-9 PF inputs but not to 3 PF inputs (**Fig. 4E**). These results suggest that input timing information coding is more sensitive to the number of PF inputs in a spine volume than in a cell volume. Indeed, when the number of PF inputs was decreased from 5 to 3, input timing information decreased only by 31.0% in a single spine, whereas it decreased by 98.6% in a cell (**Table 1**). Taken together, information coding in a spine volume was more robust against

the fluctuation of the PF amplitude and more sensitive to the low number of the PF inputs than that in a cell volume.

Spines have another important characteristic: numerosity. To investigate the advantages of the numerosity of spines, we measured the input timing information coded by multiple spines by the mutual information between the mean of the integrated Ca^{2+} over spines and PF-CF interval (**Fig. 4C**), assuming that input timing information is coded by the mean of the integrated Ca^{2+} over spines. The input timing information increased monotonically with the number of spines because the mutual information between the mean of the integrated Ca^{2+} over spines and PF-CF interval depends largely on the standard error of means of integrated Ca^{2+} , which was given by standard deviation divided by square root of the number of spines. Under the conditions with a CV of 0.1, approximately 550 spines coded as much information as a cell. Given the volume of a spine is 50,000-fold smaller than a cell, a spine can show about 90-fold mutual information per volume compared to a cell. This result indicates that numerous small spines can code more information than a single big cell.

Testable Prediction

Our results imply that the amplitude of a PF input, which corresponds to concentration of a glutamate pulse, is coded by the probability of Ca^{2+} increase in a spine volume and the amplitude of Ca^{2+} in a cell volume. This indicates that the concentration of a glutamate pulse should be observed by the number of spines with large Ca^{2+} increases in spines, whereas the integrated Ca^{2+} in a soma whose volume corresponds to a cell volume. Based on this, we propose the following testable prediction (**Fig. S4**). Based on the simulation results, we provided one of the predicted examples. With repetitive application of a glutamate pulse with the same concentration,

a similar level of Ca^{2+} increase is always expected in a soma, whereas a similar number of spines with large Ca^{2+} increase is expected in spines (**Fig. S4A**). Importantly, the spines with large Ca^{2+} increases and the amplitudes of Ca^{2+} increases in each spine are different between trials. This result will support the idea that generation of large Ca^{2+} increases in spines is stochastic rather than deterministic. Upon repetitive application of glutamate pulses of various concentrations, the number of spines with large Ca^{2+} increase and integrated Ca^{2+} in soma are predicted to increase as the concentration of glutamate increases (**Fig. S4B**). The spines with large Ca^{2+} increases are different between trials, even at the same concentration of glutamate. Thus, repetitive application of glutamate pulses at various doses to a Purkinje cell will reveal the distinct characteristics of Ca^{2+} increases in spines and the soma. Importantly, at lower doses of glutamate, large Ca^{2+} increases were observed in spines but not in the soma, indicating that spines are more sensitive to glutamate than the soma (**Fig. S4C**). This will support our finding of increased sensitivity of spines to input (**Fig. 4D-F**). The mutual information between the integrated Ca^{2+} and glutamate concentration in the stochastic simulation increased as the number of spines increased, and became comparable to that in a cell volume when the number of spines was 100,000 (**Fig. S4D**).

DISCUSSION

One of the features of our stochastic model is that the reactions and parameters of the deterministic model, which were estimated from experimental data [14], were directly used. Importantly, we created the stochastic model without changing any reactions or parameters of the deterministic model and obtained the result that the volume of real spines in Purkinje cells is optimal for probability coding. This supports the idea that the small volume of spines has been evolutionally selected based on biochemical reactions and kinetic parameters.

We provided a functional reason for the small size and numerosity of spines. The smallness of spines was optimal for probability coding of input timing information, and spines were more robust and sensitive to input than a single big cell. Many stochastic spines coded more information about input timing than a single deterministic cell. In this study, the source of fluctuation was derived from stochasticity in the number of molecules. As the number of molecules in a spine becomes smaller, the fluctuation in the number becomes larger. For example, the CVs of the Ca^{2+} indicator in a cell volume and in a spine volume are 0.003 and 0.72 at 160 msec PF-CF interval, respectively. Indeed, it has been reported that CV of the peak amplitude of dendritic Ca^{2+} transient in cerebellar Purkinje cells *in vivo* was 0.4 [20]. The fluctuation of the number of molecules is very large in a spine, suggesting that the number of molecules (amplitude) is not suitable as an information carrier. Such small numbers of molecules in a spine suggest that there may be many defective spines that do not contain essential molecules, and the reliability of a single spine is very low compared with that of a cell that contains deterministic numbers of molecules. Despite the low reliability of a single spine, summation of the probability of large Ca^{2+} increases in many spines can overcome the amplitude of Ca^{2+} in a cell in terms of the reliability of information coding. Thus, the smallness and numerosity of spines is a unique strategy for robust and sensitive information coding in neurons. Spines in other types of neurons, and small and numerous organelles may employ a similar strategy using probability coding. Our finding also raises the caution that in contrast to experiments at the scale of the cell, in experiments at the scale of a spine, the probability of signaling activities over many trials or in many spines should be measured and interpreted rather than measuring only the amplitude in a single trial in a single spine.

In this study, the input timing information was encoded into the probability of Ca^{2+} increases

in many spines. The next question is how timing-information across the spines is decoded to the final output, cerebellar LTD? Experimentally, cerebellar LTD is induced by conjunctive activation of a PF bundle and CFs, and the responses from many PF synapses are simultaneously observed [13]. Therefore, LTD in experiment is a summation of heterogeneous unitary events of LTD at many synapses, and this summation may directly corresponds to the mean of the integrated Ca^{2+} in many spines that codes input timing information (**Fig. 4**). As it has recently been reported that all-or-none LTD at many synapses can show a graded response in a stochastic situation [19,20], it is likely that cerebellar LTD show a graded bell-shaped time-window curve. Similar phenomenon has been observed in synaptic plasticity at hippocampal synapses experimentally [21,22,23].

Furthermore, the input timing information can be decoded even in LTD at a single synapse, because LTD is induced by repetitive PF and CF inputs. Three hundred times repetition of conjunctive activation of PF and CF inputs has been reported to be required for induction of maximum amplitude of LTD [24]. If 300 trials in a single spine are assumed correspond to 300 spines in the stochastic simulation, Ca^{2+} increases for cerebellar LTD can code 1.8bit information (**Fig. 4D**). Induction of cerebellar LTD has been reported to be regulated by a positive feedback loop between PKC and MAP kinase [25] and modelled all-or-none deterministic models [26]; however, it has recently been reported that cerebellar LTD can show a graded response rather than an all-or-none response in a stochastic situation [27,28]. It is likely that cerebellar LTD show a graded bell-shaped time-window curve, indicating that cerebellar LTD can decode input timing information from the frequency of Ca^{2+} increases.

The large Ca^{2+} increases are generated by the IICR system in cerebellar Purkinje cells [29,30,31]. The IICR system is an excitable system with a positive feedback loop (in which gain

is controlled by IP_3) and delayed negative feedback (**Fig. 1B**) [14]. The IICR system switches information-coding modes depending on volume; probability coding is used at spine volumes, and amplitude coding is used at cell volumes. We examined a mechanistic insight of the IICR system that generates stochastic facilitation (**Fig. S3**). Blocking the interaction of IP_3 with the IP_3 receptor, which controls the feedback gain of the regenerative cycle of Ca^{2+} , resulted in disappearance of the large Ca^{2+} increases above the threshold and decrease of the amplitude of Ca^{2+} below the threshold (**Fig. S3B**). Blocking the interaction of Ca^{2+} with the IP_3 receptor, which triggers the regenerative cycle of Ca^{2+} , resulted in disappearance of the large Ca^{2+} increases above the threshold (**Fig. S3C**). Blocking Ca^{2+} influx through the IP_3 receptor, which is responsible for regenerated increase of Ca^{2+} , resulted in the disappearance of the large Ca^{2+} increases above the threshold and decrease in the amplitude of Ca^{2+} below the threshold (**Fig. S3D**). Thus, the regenerative positive feedback loop in which gain is controlled by IP_3 appeared to be an essential mechanism for probability coding.

The IICR system is an excitable system, but its mechanism is different from that of conventional excitable systems, such as the relaxation oscillator [32]; the relaxation oscillator has a fixed threshold and stable point, whereas the IICR system has a controllable threshold and stable point. This may make a difference in a stochastic situation; however, this possibility remains to be elucidated. This makes a difference in a deterministic situation. The relaxation oscillator shows an all-or-none response with a fixed amplitude, whereas the IICR system shows a graded response with a controllable amplitude. The relaxation oscillator can transform input strength into oscillation frequency [32] rather than amplitude, whereas the IICR system can transform input strength into amplitude of Ca^{2+} increase in a cell volume. However, the IICR system has also been reported to transform growth factor concentration into the probability of

Ca^{2+} increases in some cell lines [33]. It is possible that such difference may be derived from the different bifurcation diagrams that result from the different concentrations of molecules between cell lines.

Noise-dependent enhancement of the detection of weak information-carrying signals in a threshold system is known as stochastic resonance [18]. Stochastic resonance system has been reported to enhance the system's sensitivity to weak inputs and increase ability of information transmission by the size of the system [34], which corresponds to numerosity in our study. Also, threshold-variation in stochastic resonance has been reported to increase the robustness of system output against fluctuation of input in a nanowire field-effect transistor network [35]. The sensitivity and robustness in our system may share the similar mechanisms in these systems. Our system is similar to conventional stochastic resonance; however, it has different characteristics; the source of noise is different. In stochastic resonance, noise is generally exogenous and not correlated with the signal amplitude. In contrast, in our stochastic model, noise is produced by the intrinsic stochasticity of chemical reactions and correlated with the number of molecules. Therefore, the source of fluctuation is different between stochastic facilitation in the IICR system and classical stochastic resonance. Intrinsic noise-dependent enhancement of the detection of weak information-carrying signals has recently been proposed as "stochastic facilitation" [18], and our system is another example of this.

Materials and Methods

Stochastic model

We created a stochastic simulation model of input timing-dependent Ca^{2+} increases based on the deterministic kinetic model of Ca^{2+} increases in cerebellar Purkinje cells [14]. We used the following molecules, reactions and parameters for the stochastic model (which were identical to those used for our previous deterministic model): 21 molecules, 92 reactions and 96 parameters. Among the 96 parameters, 60 parameters were determined by experiments in the deterministic kinetic model [14]. The rest of the parameters were estimated by fitting the model to the experimental data that contain information concerning the parameters [12]. Thus, the parameters in the model are likely to be biologically plausible. This model has two types of inputs: a CF input and 5 PF inputs. The CF input give a Ca^{2+} pulse (83.3 μM for 2 msec) as Ca^{2+} influx through VGCCs. The 5 PF inputs give 5 glutamate pulses (5 μM for 1 msec for each pulse) and 5 Ca^{2+} pulses (25 μM for 1 msec for each pulse) at 100 Hz, the latter of which were regarded as Ca^{2+} influx through VGCCs activated by AMPARs.

Numerical simulation

In the deterministic model, each reaction was represented as an ordinary differential equation (ODE) as was conducted in the previous model [14]. The ODEs were numerically solved by the Bogacki–Shampine method [36], a variation of Runge-Kutta method, with adaptive time step control ranging from 0.1 to 10 μsec . In the stochastic model, we discretised the ODE model based on molecular numbers. The initial numbers of molecules in the stochastic model were determined as integers based on the initial concentrations in the deterministic model.

In general, surface area of the membrane is proportional to the order of the square of length, whereas cell volume is proportional to the cube of that, which means that, as a system size increases, the increase rate of number of membrane molecules such as mGluR becomes smaller than that in cytoplasm. However, we assumed that the number of membrane proteins is proportional to the volume, *i.e.* the cube of length, throughout this study because we are interested in the influence of the smallness of the spine on the reaction system, rather than the effect of the volume-dependent changes in number ratio of membrane and cytosolic molecules.

To solve the stochastic model numerically, we utilized the modified tau-leaping method, which is an approximation of the stochastic simulation algorithm (SSA) [37]. Despite the simplicity of the method by Cao *et al.* [37], their method provides good approximations in the cases of the low-order-reaction-systems like this study [38]. We validated the use of modified tau-leaping method by comparing the results derived from modified tau-leaping method (**Fig. 2A-C**) with that derived from SSA (**Fig. S2A-C**). We repeated the same simulation with different random seeds. The number of simulation trials were as follows: 8,000 trials in the volume of $0.01 \mu\text{m}^3$, 2,000 trials in the volume of $0.1 \mu\text{m}^3$, 1,000 trials in the $0.5 \mu\text{m}^3$ and $1 \mu\text{m}^3$ volumes, 100 trials in the $10 \mu\text{m}^3$ and $100 \mu\text{m}^3$ volumes, and 20 trials in the $1,000 \mu\text{m}^3$ and $5,000 \mu\text{m}^3$ volumes. The simulation for the testable prediction was conducted 100 times. The numbers of trials were confirmed to be sufficient by resampling the simulated data (**Fig. S5D**). The simulation result in a cell volume was nearly identical to that in the previous deterministic model, supporting the validity of the stochastic model.

Decomposition of probability and amplitude components from the distribution of integrated Ca^{2+}

The integrated Ca^{2+} was defined as the temporal integration of Ca^{2+} concentration, subtracted by

the basal Ca^{2+} concentration. The probability distribution of the integrated Ca^{2+} over trials was expressed by $P(\text{Ca} | \Delta t)$ where Ca denotes the integrated Ca^{2+} , and Δt denotes the PF-CF interval, the time difference between the first PF and CF inputs. In almost all cases, the marginal distribution over PF-CF interval, $P(\text{Ca})$, was bimodal in logarithmic scale. Therefore, we set a threshold at the minimum between the two peaks of the marginal distribution (**Fig. 3A-C**, left panels).

We decomposed the distribution of the integrated Ca^{2+} into the amplitude and probability components:

$$P(\text{Ca} | \Delta t) = P(s = 0 | \Delta t)P(\text{Ca} | s = 0, \Delta t) + P(s = 1 | \Delta t)P(\text{Ca} | s = 1, \Delta t), \quad (1)$$

where $s = 1$ represents that the integrated Ca^{2+} exceeded the threshold, and $s = 0$ otherwise (**Fig. 2D**). In this representation, $P(s | \Delta t)$ and $P(\text{Ca} | s, \Delta t)$ corresponds to the probability and amplitude component, respectively. The probability component, $P(s | \Delta t)$, gives the probabilities of the integrated Ca^{2+} above/below the threshold, and the amplitude component, $P(\text{Ca} | s, \Delta t)$, gives the probability distributions of the integrated Ca^{2+} , partitioned by the threshold.

Calculation of input timing information

We measured the input timing information coded by the integrated Ca^{2+} as mutual information between the integrated Ca^{2+} and PF-CF interval:

$$I_{total} = \sum_{\Delta t} P(\Delta t) \int_{\text{Ca}} P(\text{Ca} | \Delta t) \log_2 \frac{P(\text{Ca} | \Delta t)}{P(\text{Ca})} d\text{Ca}. \quad (2)$$

Here, $P(\Delta t)$ follows the uniform distribution, and Δt denotes the PF-CF interval ($\Delta t = -400, -380, -360, \dots, +600$ msec), and the integrated Ca^{2+} , Ca , was partitioned into bins where the bin width was fixed at 0.05 in logarithmic scale with base 10. We also measured the information coded by the probability component by use of the Kullback–Leibler (KL) divergence:

$$I_{probability} = \sum_{\Delta t} P(\Delta t) \int_{Ca} P(Ca | \Delta t) \log_2 \frac{P(Ca | \Delta t)}{P_{-probability}(Ca | \Delta t)} dCa, (3)$$

where $P_{-probability}(Ca | \Delta t)$ denotes the distribution of the integrated Ca^{2+} without the probability component, which was calculated by marginalizing Δt out of the probability component $P(s | \Delta t)$ in $P(Ca | \Delta t)$:

$$P_{-probability}(Ca | \Delta t) = P(s = 0)P(Ca | s = 0, \Delta t) + P(s = 1)P(Ca | s = 1, \Delta t). (4)$$

Further, we measured the information coded by the amplitude component:

$$I_{amplitude} = \sum_{\Delta t} P(\Delta t) \int_{Ca} P(Ca | \Delta t) \log_2 \frac{P(Ca | \Delta t)}{P_{-amplitude}(Ca | \Delta t)} dCa, (5)$$

where $P_{-amplitude}(Ca | \Delta t)$ denotes the distribution of the integrated Ca^{2+} without the amplitude component, which was calculated by marginalizing Δt out of the amplitude component $P(Ca | s, \Delta t)$ in $P(Ca | \Delta t)$:

$$P_{-amplitude}(Ca | \Delta t) = P(s = 0 | \Delta t)P(Ca | s = 0) + P(s = 1 | \Delta t)P(Ca | s = 1). (6)$$

Here, the sum of $I_{probability}$ and $I_{amplitude}$ is equal to I_{total} . The relative contributions of the probability and amplitude components to the input timing information were defined by

$I_{probability}/I_{total}$ and $I_{amplitude}/I_{total}$, respectively.

Fluctuation of PF input amplitude

For fluctuation of PF input amplitudes, the concentration of 5 glutamate pulses and 5 Ca^{2+} pulses fluctuated between trials under the fixed mean concentration (5 μM). The fluctuation of PF input amplitudes follows the zero-truncated normal distribution with a given coefficient of variation where the PF input amplitude must be over zero.

Input timing information coded by multiple spines.

In the simulation with spines, we assumed that input timing information was coded by the mean

integrated Ca^{2+} over spines:

$$\langle Ca \rangle = \frac{1}{N} \sum_{i=1}^N Ca_i, \quad (7)$$

where N denotes the number of spines, and Ca_i denotes the integrated Ca^{2+} in i^{th} spine. We measured the input timing information coded by multiple spines by use of the mutual information between the mean integrated Ca^{2+} over spines and PF-CF interval. Since Ca^{2+} increases are assumed to independently occur in identical spines, the mean integrated Ca^{2+} over multiple spines, $\langle Ca \rangle$, is equivalent to that over multiple trials in a single spine.

Acknowledgements: We thank Keiko Tanaka (KIST, Korea) for providing the image of cerebellar Purkinje cells and critically reading this manuscript. We also thank our laboratory members for critically reading this manuscript and their technical assistance with the simulation. The stochastic and deterministic models have been placed on our website (http://www.kurodalab.org/info/Ca_Increases).

REFERENCES

1. Napper RM, Harvey RJ (1988) Number of parallel fiber synapses on an individual Purkinje cell in the cerebellum of the rat. *J Comp Neurol* 274: 168-177.
2. Stuart G, Spruston N, Häusser M (1999) *Dendrites*. Oxford: Oxford University Press.
3. Harris KM, Stevens JK (1988) Dendritic spines of rat cerebellar Purkinje cells: serial electron microscopy with reference to their biophysical characteristics. *J Neurosci* 8: 4455-4469.
4. Rapp M, Segev I, Yarom Y (1994) Physiology, morphology and detailed passive models of guinea-pig cerebellar Purkinje cells. *J Physiol* 474: 101-118.
5. Takacs J, Hamori J (1994) Developmental dynamics of Purkinje cells and dendritic spines in rat cerebellar cortex. *J Neurosci Res* 38: 515-530.
6. Ito M (1970) Neurophysiological aspects of the cerebellar motor control system. *Int J Neurol* 7: 162-176.
7. Kawato M (1999) Internal models for motor control and trajectory planning. *Curr Opin Neurobiol* 9: 718-727.
8. Kawato M, Kuroda S, Schweighofer N (2011) Cerebellar supervised learning revisited: biophysical modeling and degrees-of-freedom control. *Curr Opin Neurobiol* 21: 791-800.
9. Mauk MD, Garcia KS, Medina JF, Steele PM (1998) Does cerebellar LTD mediate motor learning? Toward a resolution without a smoking gun. *Neuron* 20: 359-362.
10. Steinmetz JE (1990) Classical nictitating membrane conditioning in rabbits with varying interstimulus intervals and direct activation of cerebellar mossy fibers as the CS. *Behav Brain Res* 38: 97-108.
11. Miyakawa H, Lev-Ram V, Lasser-Ross N, Ross WN (1992) Calcium transients evoked by climbing fiber and parallel fiber synaptic inputs in guinea pig cerebellar Purkinje neurons. *J Neurophysiol* 68: 1178-1189.
12. Wang SS, Denk W, Häusser M (2000) Coincidence detection in single dendritic spines mediated by calcium release. *Nat Neurosci* 3: 1266-1273.
13. Ito M (2002) The molecular organization of cerebellar long-term depression. *Nat Rev Neurosci* 3: 896-902.
14. Doi T, Kuroda S, Michikawa T, Kawato M (2005) Inositol 1,4,5-trisphosphate-dependent Ca^{2+} threshold dynamics detect spike timing in cerebellar Purkinje cells. *J Neurosci* 25: 950-961.
15. Bhalla US (2004) Signaling in small subcellular volumes. II. Stochastic and diffusion effects on synaptic network properties. *Biophys J* 87: 745-753.
16. Bhalla US (2004) Signaling in small subcellular volumes. I. Stochastic and diffusion effects on individual pathways. *Biophys J* 87: 733-744.
17. Komorowski M, Costa MJ, Rand DA, Stumpf MP (2011) Sensitivity, robustness, and identifiability in stochastic chemical kinetics models. *Proc Natl Acad Sci USA* 108: 8645-8650.
18. McDonnell MD, Ward LM (2011) The benefits of noise in neural systems: bridging theory and experiment. *Nat Rev Neurosci* 12: 415-426.
19. Barbour B (1993) Synaptic currents evoked in Purkinje cells by stimulating individual granule cells. *Neuron* 11: 759-769.
20. Kitamura K, Häusser M (2011) Dendritic calcium signaling triggered by spontaneous and sensory-evoked climbing fiber input to cerebellar Purkinje cells in vivo. *J Neurosci* 31: 10847-10858.

21. Enoki R, Hu YL, Hamilton D, Fine A (2009) Expression of long-term plasticity at individual synapses in hippocampus is graded, bidirectional, and mainly presynaptic: optical quantal analysis. *Neuron* 62: 242-253.
22. O'Connor DH, Wittenberg GM, Wang SS (2005) Graded bidirectional synaptic plasticity is composed of switch-like unitary events. *Proc Natl Acad Sci USA* 102: 9679-9684.
23. Petersen CC, Malenka RC, Nicoll RA, Hopfield JJ (1998) All-or-none potentiation at CA3-CA1 synapses. *Proc Natl Acad Sci USA* 95: 4732-4737.
24. Karachot L, Kado RT, Ito M (1994) Stimulus parameters for induction of long-term depression in in vitro rat Purkinje cells. *Neurosci Res* 21: 161-168.
25. Tanaka K, Augustine GJ (2008) A positive feedback signal transduction loop determines timing of cerebellar long-term depression. *Neuron* 59: 608-620.
26. Kuroda S, Schweighofer N, Kawato M (2001) Exploration of signal transduction pathways in cerebellar long-term depression by kinetic simulation. *J Neurosci* 21: 5693-5702.
27. Antunes G, De Schutter E (2012) A stochastic signaling network mediates the probabilistic induction of cerebellar long-term depression. *J Neurosci* 32: 9288-9300.
28. De Schutter E (2012) The importance of stochastic signaling processes in the induction of long-term synaptic plasticity. *Neural Netw.*
29. Berridge MJ (1998) Neuronal calcium signaling. *Neuron* 21: 13-26.
30. Finch EA, Augustine GJ (1998) Local calcium signaling by inositol-1,4,5-trisphosphate in Purkinje cell dendrites. *Nature* 396: 753-756.
31. Inoue T, Kato K, Kohda K, Mikoshiba K (1998) Type 1 inositol 1,4,5-trisphosphate receptor is required for induction of long-term depression in cerebellar Purkinje neurons. *J Neurosci* 18: 5366-5373.
32. Tsai TY, Choi YS, Ma W, Pomerening JR, Tang C, et al. (2008) Robust, tunable biological oscillations from interlinked positive and negative feedback loops. *Science* 321: 126-129.
33. Thomas AP, Bird GS, Hajnoczky G, Robb-Gaspers LD, Putney JW, Jr. (1996) Spatial and temporal aspects of cellular calcium signaling. *FASEB J* 10: 1505-1517.
34. Collins JJ, Chow CC, Imhoff TT (1995) Stochastic resonance without tuning. *Nature* 376: 236-238.
35. Kasai S, Miura K, Shiratori Y (2010) Threshold-variation-enhanced adaptability of response in a nanowire field-effect transistor network. *Applied Physics Letters* 96.
36. Bogacki P, Shampine LF (1989) A 3(2) pair of Runge - Kutta formulas. *Appl Math Lett* 2: 321-325.
37. Cao Y, Gillespie DT, Petzold LR (2006) Efficient step size selection for the tau-leaping simulation method. *J Chem Phys* 124: 044109.
38. Gillespie DT, Hellander A, Petzold LR (2013) Perspective: Stochastic algorithms for chemical kinetics. *J Chem Phys* 138: 170901

Figure Legends

Figure 1. Ca^{2+} increase in cerebellar Purkinje cells. **A**, Cerebellar Purkinje cells. Male mouse cerebellar Purkinje cells were doubly stained with anti-calbindin antibody to visualize whole cells (green) and with anti-mGluR (metabotropic glutamate receptor) antibody to specifically visualize the spines of the PF-Purkinje cell synapses (red). The inset in the left image is magnified in the right panel. The average volume of spines in cerebellar Purkinje cells has been reported to be $0.1 \mu\text{m}^3$, which is 10^4 -fold smaller than a cell body ($5,000 \mu\text{m}^3$). White circles in the left and right panels indicate a typical soma and spine, respectively. **B**, Schematic representation of PF and CF inputs-dependent Ca^{2+} increase in the simulation model[14] (Materials and Methods). Abbreviations: Glu; glutamate, mGluR; metabotropic glutamate receptor, IP_3 ; inositol trisphosphate; AMPAR; α -amino-3-hydroxy-5-methyl-4-isoxazole propionic acid receptor, VGCC; voltage-gated Ca^{2+} channels. Parentheses indicate initial numbers of the indicated molecules in the stochastic model. **C**, Ca^{2+} responses along the PF-CF interval in the experiments (black circles)[12], and mean Ca^{2+} responses in the stochastic simulation in a spine volume ($0.1 \mu\text{m}^3$) (solid line) and in the stochastic simulation in a cell volume ($5,000 \mu\text{m}^3$) (dashed line). The Ca^{2+} response was defined as the average relative change in fluorescence ($\Delta F/F_0$) of Magnesium Green 1, a Ca^{2+} indicator[14]. Positive sign of the interval are given to Δt msec when PF inputs precede CF inputs; otherwise, a negative sign is given. Five PF inputs at 100Hz and a single CF were given.

Figure 2. Ca^{2+} increases in the stochastic model. **A, B**, Ca^{2+} increase due to stimulation of PF and CF inputs with $\Delta t = 160$ msec (**A**) and $\Delta t = -400$ msec (**B**) in the stochastic model in a spine volume (gray lines, $n=2,000$ for each timing, 20 examples are shown) and in a cell volume (black

lines, $n=20$ for each timing). **C**, Distributions of the integrated Ca^{2+} in a spine volume with $\Delta t = 160$ msec (solid line) and $\Delta t = -400$ msec (dashed line). Solid and dashed arrowheads indicate the means of the integrated Ca^{2+} in a cell volume with $\Delta t = 160$ msec and $\Delta t = -400$ msec, respectively. Note that y-axis has a logarithmic scale, and that Ca^{2+} increases in a cell volume were almost the same between trials, leading to the overlap of the time courses (**A**, **B**). **D**, The distribution of the integrated Ca^{2+} (upper panel) was divided into the distribution with Ca^{2+} spikes ($s=1$, black) and the distribution without Ca^{2+} spikes ($s=0$, gray with dashed line). Then, each right ($s=1$) and left ($s=0$) distribution is decomposed into the probability components, which is probability of Ca^{2+} spiking (middle panel), and amplitude components, which is distribution of the integrated Ca^{2+} conditioned by Ca^{2+} spiking (lower panel). See materials and methods for the detailed descriptions.

Figure 3. Volume-dependent time window of Ca^{2+} increases. **a-c**, Distributions of the integrated Ca^{2+} along the PF-CF interval (left) in $0.1 \mu\text{m}^3$ (a spine volume) (**A**), in $5,000 \mu\text{m}^3$ (a cell volume) (**B**), and in $0.01 \mu\text{m}^3$ (**C**). The probability components (middle) and the amplitude components (right) are also shown. The colors in the left and right panels code the probability density of the integrated Ca^{2+} in logarithmic scale at the indicated PF-CF interval. Arrowheads in the left panels indicate the thresholds between two peaks of the bimodal marginal distributions. The probability components denote the frequencies of the integrated Ca^{2+} above/below the thresholds (solid/dashed lines, respectively), and the amplitude components denote the integrated Ca^{2+} above/below the thresholds (solid/dashed lines, respectively). The PF-CF interval was defined by the time difference between the first PF and CF inputs. **D**, Volume-dependency of the input timing information coded by the total distribution of the integrated Ca^{2+} (black), by the

probability component (red), and by the amplitude component (blue). **E**, Relative contribution of the probability (red) and amplitude (blue) component to the input timing information.

Figure 4. Robust and sensitive probability coding in the stochastic model. A, B, Mean \pm standard deviation of the integrated Ca^{2+} in a single spine (**A**) and in a cell (**B**) due to stimulation of PF and CF inputs with fluctuating the PF amplitudes between trials. The mean and standard deviation of the integrated Ca^{2+} are indicated by solid and dashed lines, respectively. CVs of the PF amplitudes were 0.1 (black) and 0.5 (red). **C**, Input timing information coded by the integrated Ca^{2+} in a single spine (light blue), 10 spines (blue), 100 spines (green), and 100 spines (light green) and in a cell (black). Note that all spines are identical and independently generate Ca^{2+} increases in the stochastic model. **D, E**, Mean \pm standard deviation of the integrated Ca^{2+} in a single spine (**D**) and in a cell (**E**) with a single PF input (black, bottom), 3 PF inputs, 5 PF inputs, 7 PF inputs, and 9 PF inputs (red, top). CV of the PF amplitudes was 0.1. The mean and standard deviation of the integrated Ca^{2+} are indicated by solid and dashed lines, respectively. **F**, Input timing information coded by the integrated Ca^{2+} in a spine volume with a single spine, 10 spines, 100 spines, and 1,000 spines and in a cell volume. The colors were the same as in **C**.

# of spines or a cell	Decrease of the input timing information	
	CV of PF amplitude from 0.05 to 0.5	# of PF inputs from 5 to 3
1 spine	10.1%	31.0%
10 spines	10.3%	21.7%
100 spines	6.6%	20.6%
1,000 spines	1.3%	9.4%
a cell	77.3%	98.6%

Table 1. Decrease of the input timing information with the change of the CV of PF amplitude from 0.05 to 0.5 and the number of PF inputs from 5 to 3.

Supporting Information Legends

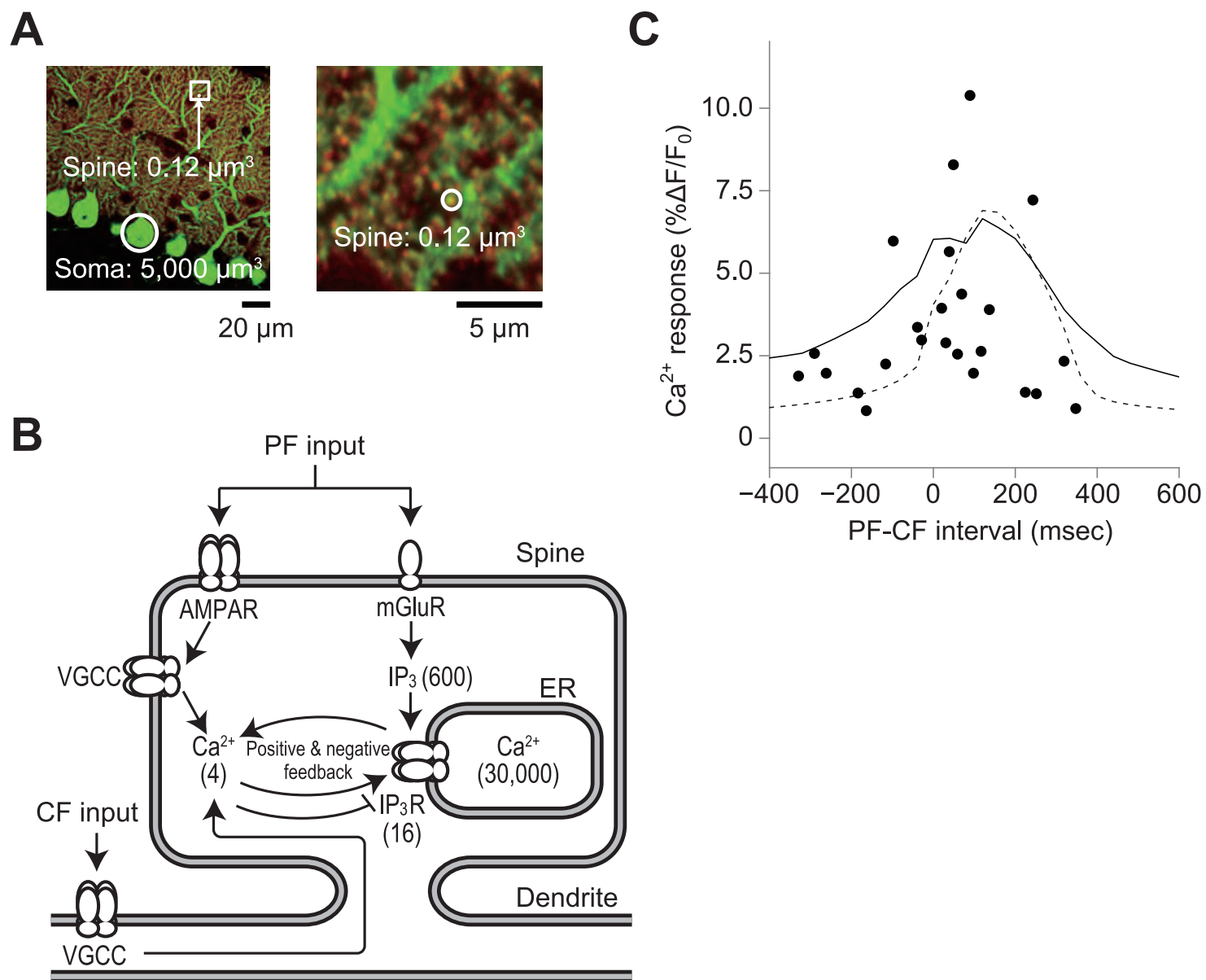
Figure. S1 | Time courses of concentrations of inositol trisphosphate (IP₃) and Ca²⁺ in the endoplasmic reticulum (ER). **A, B,** Time courses of concentrations of IP₃ in response to PF and CF inputs with $\Delta t = 160$ msec (**A**) and $\Delta t = -400$ msec (**B**) in the stochastic model in a spine volume (gray lines, $n=2,000$ for each timing, 20 examples are shown) and in a cell volume (black lines, $n=20$ for each timing), respectively. **C, D,** Time courses of concentrations of Ca²⁺ in the ER in response to PF and CF inputs with $\Delta t = 160$ msec (**C**) and $\Delta t = -400$ msec (**D**) in the stochastic model in a spine volume (gray lines, $n=2,000$ for each timing, 20 examples are shown) and in a cell volume (black lines, $n=20$ for each timing), respectively.

Figure. S2 | Distribution of integrated Ca²⁺ and that without the probability and/or amplitude components. **A,** Distribution of integrated Ca²⁺. **B, C,** Distribution of integrated Ca²⁺ without probability (**B**) or amplitude (**C**) component. **D,** Distribution of integrated Ca²⁺ without both components. Input timing information coded by the probability and amplitude component was calculated by the Kullback–Leibler (KL) divergence of the distribution of **B** and **C** from that of **A**, respectively. Input timing information coded by the distribution of integrated Ca²⁺ was calculated by the mutual information between integrated Ca²⁺ and PF-CF interval, which is equal to the KL divergence of the distribution of **D** from that of **A**, and also equal to the sum of the input timing information coded by probability and amplitude component.

Figure. S3 | Mechanism of probability coding. **A**, Schematic representation of the pathway deleted in the following figures. **B-D**, Distribution of integrated Ca^{2+} along the PF-CF interval in a spine volume with blocking of the interaction of IP_3 with the IP_3 receptor (**B**), with blocking of the interaction of Ca^{2+} with the IP_3 receptor (**C**), and with blocking of Ca^{2+} influx through the IP_3 receptor (**D**) in the stochastic simulation. **E**, Distribution of integrated Ca^{2+} without deletion (control).

Figure. S4 | Possible experimental tests of probability coding in spines and amplitude coding in a soma. **A**, Ca^{2+} increase in response to repetitive addition of glutamate pulses with the same concentration in the stochastic model (spines) and in the deterministic model (soma). Colours code the concentration of Ca^{2+} . Darker colours indicate higher concentrations of Ca^{2+} . The time course of Ca^{2+} increase in the deterministic model and stochastic model are shown. **B**, Ca^{2+} increases in response to glutamate pulses of various concentrations in the stochastic model (spines) and the deterministic model (soma). Darker colours indicate higher concentrations of Ca^{2+} . The time course of Ca^{2+} increase in the deterministic model and stochastic model are shown. **C**, Glutamate dose-responses curves of the fraction of spines with large Ca^{2+} increase above the threshold in the stochastic model (solid lines) and integrated Ca^{2+} in the deterministic model (dashed lines). Note glutamate inputs with amplitude CVs of 0.1 were used. **D**, The information on input (glutamate) doses coded by the integrated Ca^{2+} in the stochastic model (line) and in the deterministic model (arrow). The information was calculated by the mutual information between the integrated Ca^{2+} and glutamate doses.

Figure. S5 | Validation of the numerical simulation. A, B, Ca^{2+} increase due to stimulation of PF and CF inputs with $\Delta t = 160$ msec (**A**) and $\Delta t = -400$ msec (**B**) by the stochastic simulation algorithm (SSA) (gray lines, $n=2,000$ for each timing, 20 examples are shown). **C,** Distributions of the integrated Ca^{2+} in a spine volume with $\Delta t = 160$ msec (solid lines) and $\Delta t = -400$ msec (dashed line) by the modified tau-leaping method (black lines, same as **Fig. 2C**) and SSA (red lines). The similarity of the red and black lines demonstrates the validity of the modified tau-leaping method. **D,** to confirm the sufficiency of the numbers of simulation trials, we calculated the mutual information between the integrated Ca^{2+} and PF-CF interval by jackknifing (i.e. for the data resampled randomly without replacement). We calculated the mutual information for the 20 data sets consisting of the quarter and the half of the whole data (grey and black lines, respectively). The red line indicates the mutual information for the original data (same as **Fig. 3D**, black line). The variance of the mutual information for the data sets consisting of the half of the whole data was smaller than that for the data sets consisting of the quarter, which was almost the same as that for the original data, indicating that the numbers of the original data were sufficient.



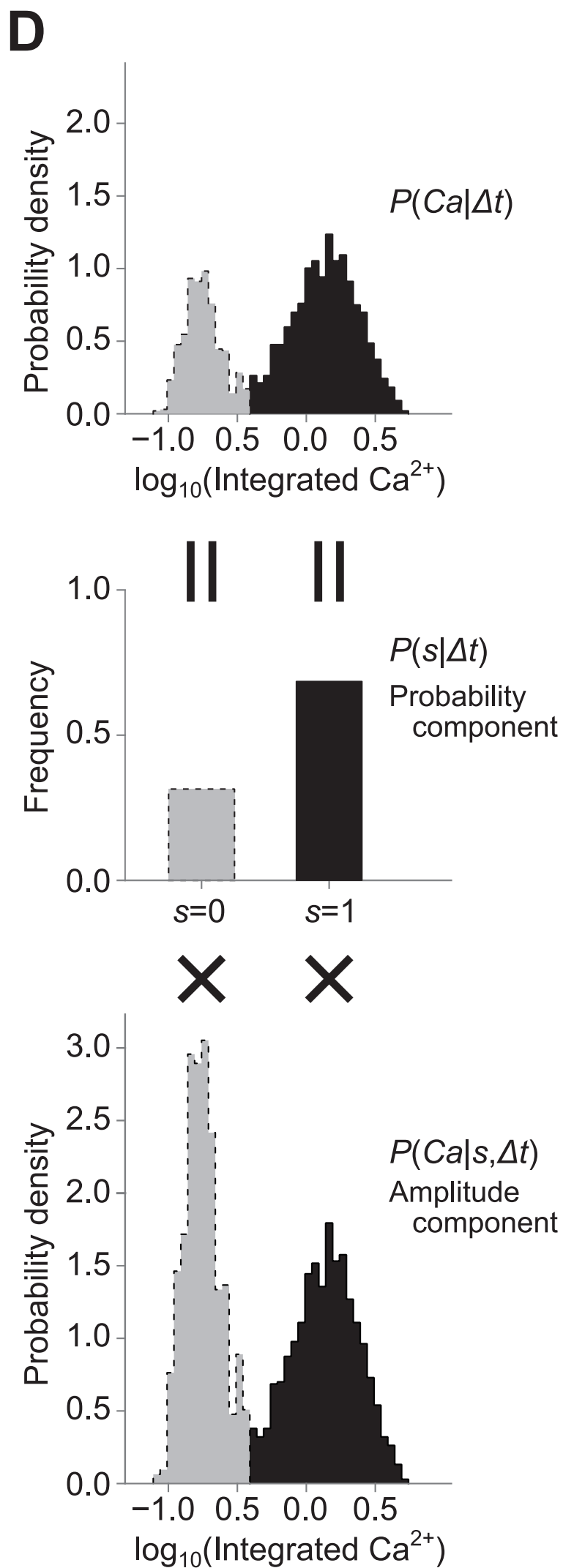
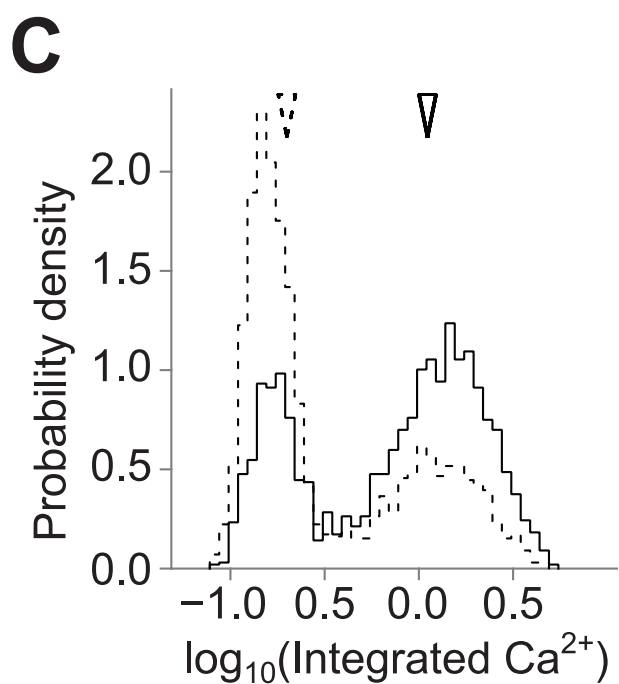
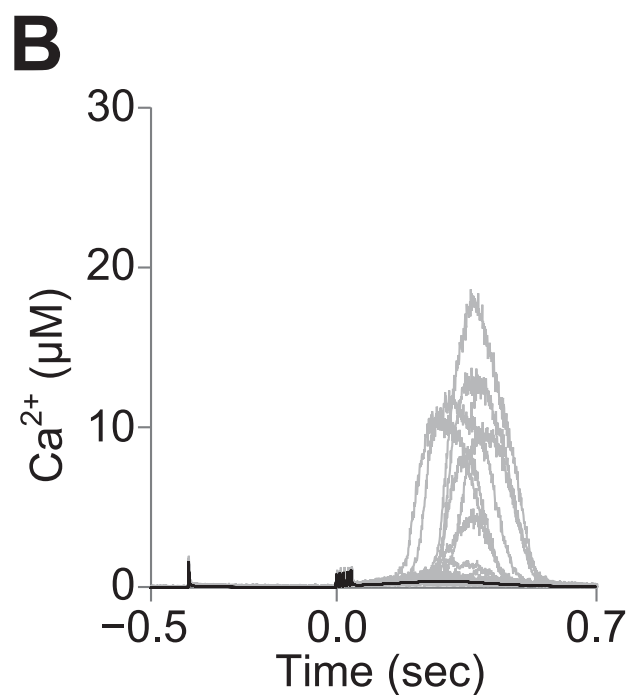
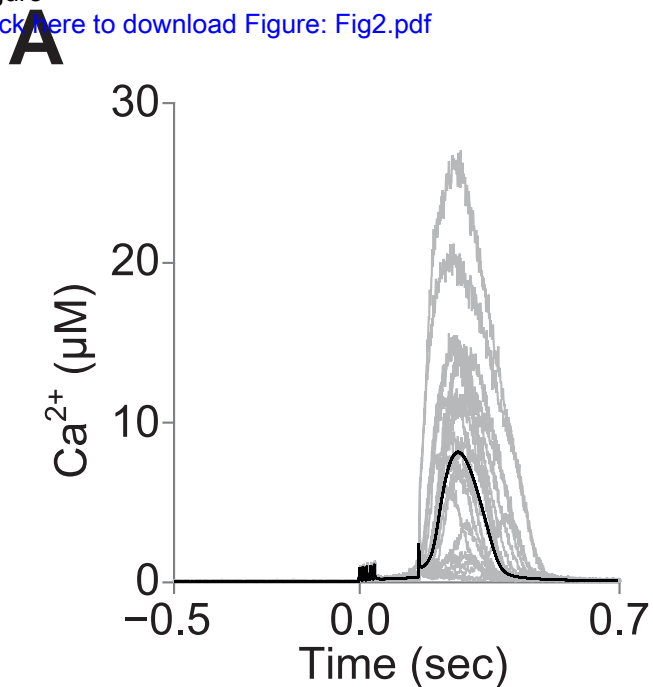
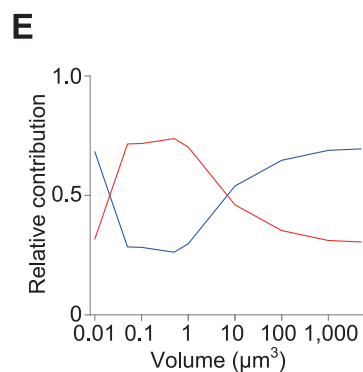
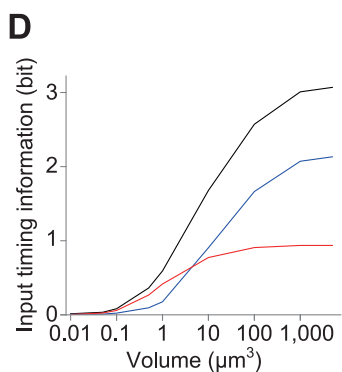
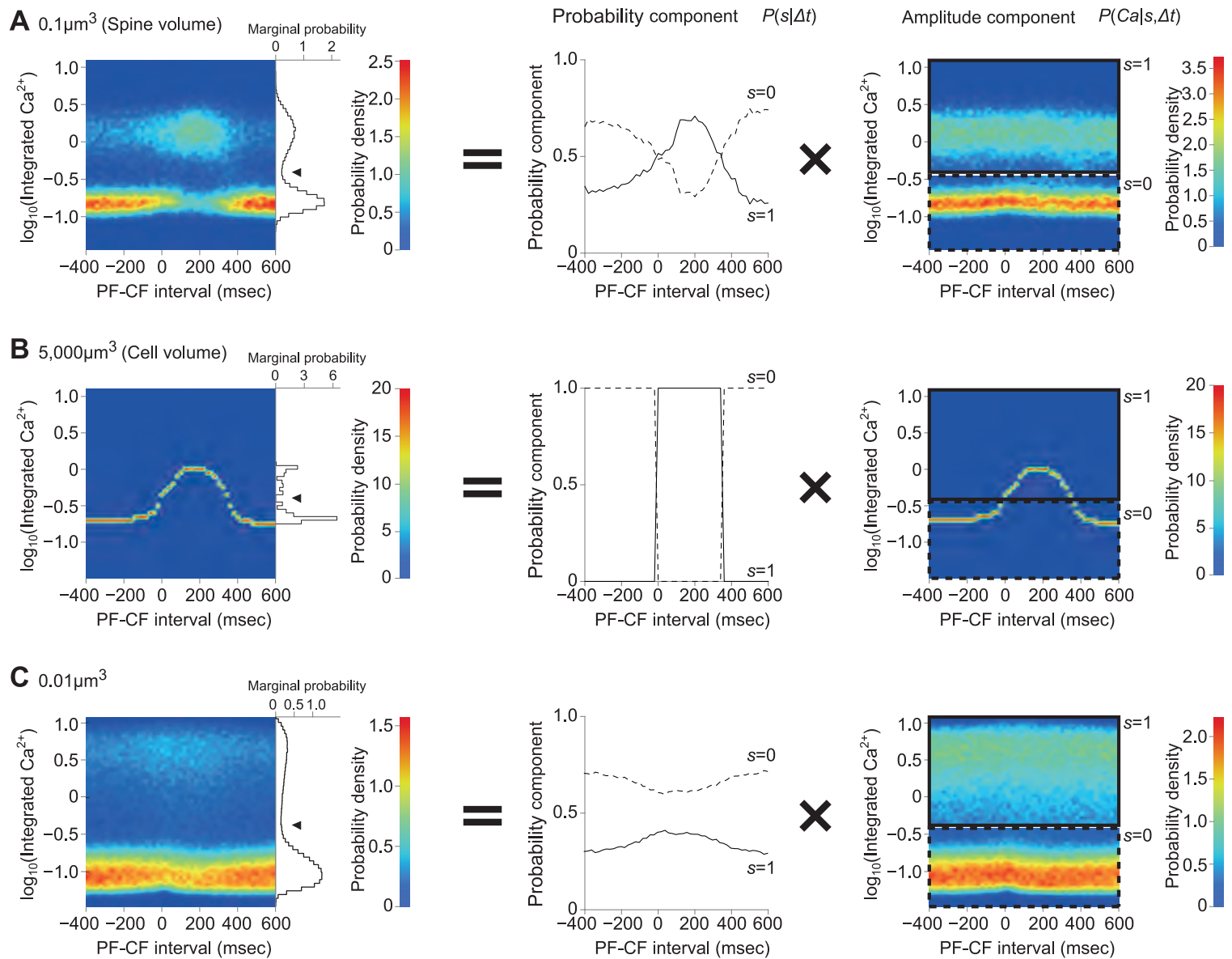
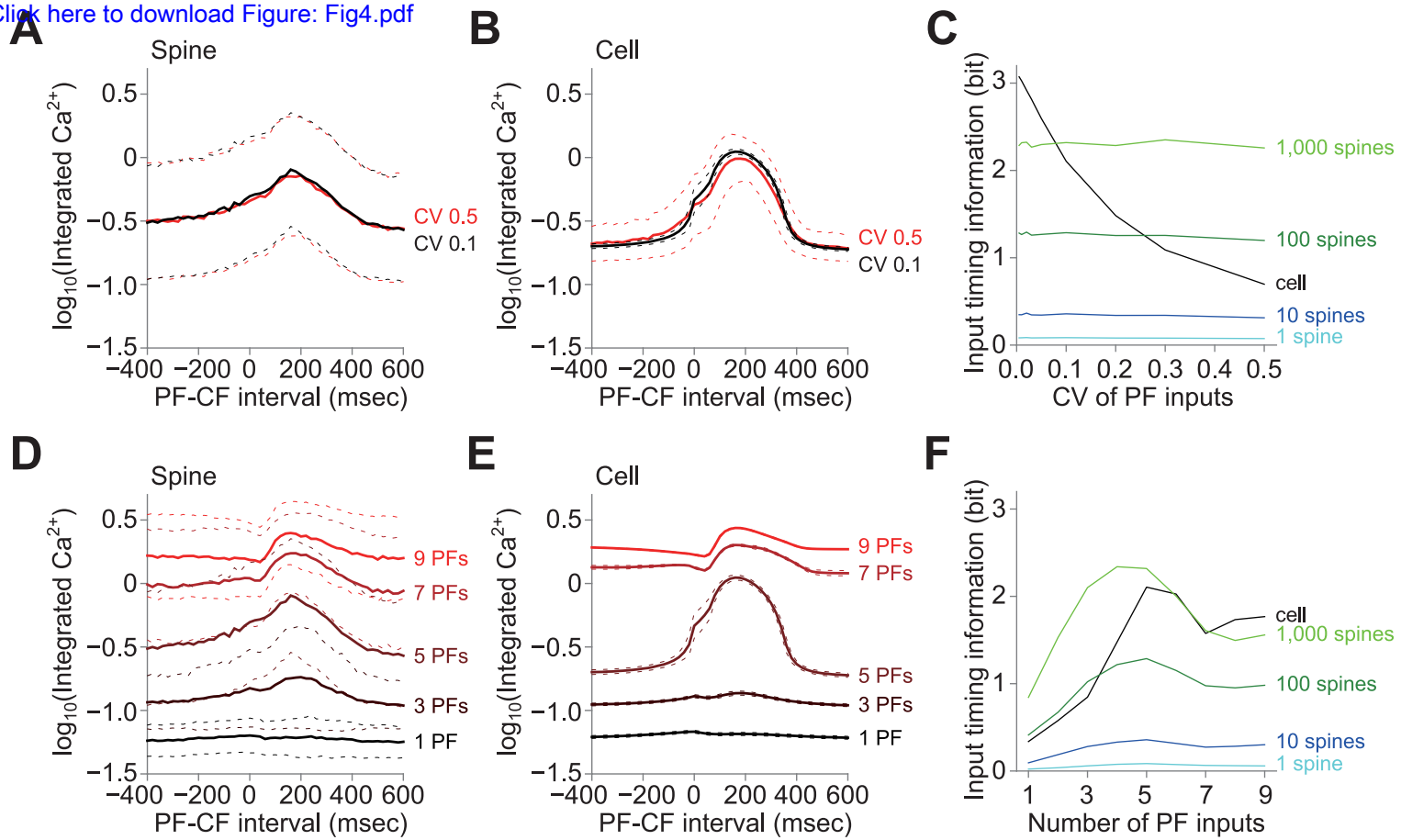


Figure
[Click here to download Figure: Fig3.pdf](#)





Supporting Information

[Click here to download Supporting Information: FigS1.pdf](#)

Supporting Information

[Click here to download Supporting Information: FigS2.pdf](#)

Supporting Information

[Click here to download Supporting Information: FigS3.pdf](#)

Supporting Information

[Click here to download Supporting Information: FigS4.pdf](#)

Supporting Information

[Click here to download Supporting Information: FigS5.pdf](#)